The Impact of Atmosphere on Energetics of Lead Halide Perovskites

The impact of atmosphere on energetics of lead halide perovskites

Zhanhao Hu, Zonghao Liu, Luis K. Ono, Maowei Jiang, Sisi He, Dae-Yong Son, and Yabing Qi*

Dr Z. Hu, Dr Z. Liu, Dr L. K. Ono, Dr M. Jiang, Dr S. He, Dr D.-Y. Son, Prof. Y.B. Qi
Energy Materials and Surface Sciences Unit (EMSSU), Okinawa Institute of Science and Technology Graduate University (OIST), 1919-1 Tancha, Onna-son, Kunigami-gun, Okinawa 904-0495, Japan.
E-mail: Yabing.Qi@OIST.jp

Solar cells based on metal halide perovskites have emerged as a promising low-cost photovoltaic technology. In contrast to inert atmosphere where most of the lab-scale devices are made to date, large-area low-cost production of perovskite solar cells often involves processing of perovskites in various atmospheres including ambient air, nitrogen and / or vacuum. Herein, we systematically investigated the impact of atmosphere on the energy levels of methylammonium lead halide perovskite films. The atmosphere is varied to simulate the typical fabrication process. Through a comprehensive analysis combining the Fermi level evolution, surface photovoltage, photoluminescence property, photovoltaic performance and device simulation, we are able to determine an overall landscape of the energy diagram of the perovskite layer. Our findings have direct implications for real-world devices under typical atmospheres, and provide insights into the fabrication-process design and optimization. Furthermore, a universal Fermi level shift under vacuum for lead-halide based perovskites revealed in this study urges a refreshed view on the energetics studies conducted without considering the atmospheric effect.

1. Introduction

In recent years, solar cells based on lead halide perovskites have emerged as a competitive alternative to the market-dominating silicon based solar cells[1]. A precise knowledge of the optoelectronic properties of the perovskite is imperative to attain photovoltaic performance near the Shockley-Queisser limit[2]. Furthermore, an understanding of how the energy levels align at the perovskite/charge collection material interfaces helps determine the best combination of the film stacks to minimize energy loss and improve charge transport throughout the device. However, a general model for the energy level alignment of perovskites has yet to be established. The difficulty could be ascribed to the complex intertwined factors, such as composition, processing, substrates, etc., which affect perovskite's energetics. For example, composition of the best-known methylammonium lead iodide (MAPbI$_3$) has been found to influence its semiconductor type. Deviation from the MA : Pb : I = 1 : 1 : 3 stoichiometry was found to induce self-doping through generation of defect states near band edges[3,4]. The substrate on which the perovskite is deposited was also reported to affect its Fermi level (E_f) position[5,6]. Furthermore, formation of a dipole layer and band bending near the bottom substrate/perovskite interface has been revealed by incremental depositions of MAPbI$_3$ in vacuum[7]. E_f on the surface is thus also related with the specific perovskite film thickness.

Recently, atmospheric effect on the photoluminescence of the perovskite has been reported[8–11]. It was found that oxygen and water molecules can passivate the prevalent halide vacancies, leading to an increased photoluminescence efficiency. Impact of atmosphere on the energy levels, however, was rarely studied. The potential atmospheric effect has significant implications on device fabrication. During a common fabrication procedure of solar cells in the lab, the perovskite film is subjected to a variety of atmospheres before encapsulation, i.e., ambient air and/or N$_2$ environment amid solution processing, and vacuum during back electrode evaporation. On the other hand, on a mass production line in a factory, all the procedures except electrode deposition is conducted in air[12]. If carbon is further employed as the back electrode, full-air processing becomes possible without ever transferring the sample into vacuum[13]. Yet, our current understanding on the energetic properties of perovskite materials is mainly built upon studies conducted in high vacuum, especially those by photoemission spectroscopy (PES). It is thus urgent to examine how much of the knowledge holds for perovskites subjected to other atmospheres relevant to device fabrication.

To the best of our knowledge, the first study that compared the energy level under different atmospheres was the report by Cahen et al[14]. A drastic shift of E_f towards the conduction band minimum (CBM) was observed when transferring MAPbI$_3$(Cl) thin film into vacuum (~ 10^{-1} Pa). However, it is still difficult to draw a clear picture of the energy level landscape from these studies[14–17]. For example, very few studies have compared perovskite films prepared on different substrates, which have been proposed to p- or n-dope the perovskite; it is unclear whether the energy level shift is limited on the surface or extended into the film bulk; it is difficult to predict whether the conclusions drawn from these studies can be applied to the real-world devices because the measurement environment is not systematically controlled to simulate the real fabrication process.

Herein, we conducted a series of controlled experiments to study the impact of atmosphere on the energy levels of MAPbI$_3$. Specifically, we focus on the high quality MAPbI$_3$(Cl) which is the typical formulation for photovoltaic applications and offers a high power-conversion efficiency. A minor addition of Cl improves the crystal quality and allows deposition of thick films with full coverage and large grains, which thus ensures that the experimental results obtained on thick films are more relevant to the intrinsic property of the perovskite[18]. The thin films are prepared on the n-type TiO$_2$ and p-type poly(3,4-ethylenedioxythiophene) polystyrene sulfonate (PEDOT:PSS) substrates by a solution process. Non-destructive Kelvin

probe measurements are performed to obtain the intrinsic work function of perovskite films, which corresponds to the Fermi level position relative to the vacuum level. The sample is subjected to a cycle of atmospheres relevant to device fabrication under the ambient air, N_2 and vacuum ($10^{-3} \sim 10^{-4}$ Pa). The overall landscape of the energy diagram of the perovskite is obtained by a combination study on the thickness-dependent E_f, surface photovoltage (SPV) and photoluminescence characteristics. It is found that MAPbI$_3$(Cl) behaves as a low-doped intrinsic semiconductor in air and the energy diagram follows the vacuum-level-alignment model. Transferring the perovskite inside dry N_2 atmosphere does not modify E_f from the previous atmosphere. However, when pumped into vacuum, MAPbI$_3$(Cl) becomes highly n-doped with its E_f shifting toward CBM. Implications of the doping transition on the photovoltaic performance is further explored by electrical characterizations and device simulation. The universal vacuum-induced n-doping found in various perovskite formulations based on lead-halide calls for a refreshed view on the energetics studies conducted without considering the atmospheric effect.

2. Results and discussion

2.1. Set-up of the Kelvin Probe Measurement

Most studies in the literature have employed PES for obtaining the energy level information

of perovskites. PES is commonly operated in ultra-high vacuum and is capable of acquiring

the valence band maximum (VBM) and work function with minimal contamination from

ambient air. However, when considering devices in practical production, the semiconductor

thin films are subjected to various atmospheres during fabrication as well as under operation.

It is thus important to investigate how much the energy level may change under these

atmospheres. Another limitation of PES is that the ultraviolet-induced or X-ray-induced

photo-charges may alter band bending inside the sample through the SPV effect and thus the

information on the E_f position could be distorted[19,20]. To enable characterization in different

atmospheres and avoid artifacts from excitation probes (e.g., X-ray, ultraviolet) on the sample,

a Kelvin-probe set-up inside a vacuum chamber as shown in **Figure 1**a is employed. The

installed vacuum pump is able to produce a high vacuum ($10^{-3} \sim 10^{-4}$ Pa), which is the same

level as that in a typical electrode deposition chamber during device fabrication. The chamber

can also be vented with dry N_2 or ambient air (temperature ~ 24 °C, relative humidity ~ 40 %)

through a gas valve to simulate transferring of the sample to the N_2 atmosphere in a glove-box

as well as out to the air. The full measurement flow is illustrated in Figure 1b. In addition, two light-emitting diodes (LEDs) emitting at 627 nm are set above and below the sample to induce SPV. The Kelvin probe is calibrated to determine the absolute work function of the sample. For each experimental condition examined in this study, more than three samples were measured to confirm the reproducibility. Variation within $\pm$ 0.1 eV was generally observed, and is considered in the data analysis.

2.2. Atmospheric Effect

MAPbI$_3$(Cl) was prepared in ambient air by a simple solution process reported in our earlier work[18]. The method produces high-quality perovskite thin films as confirmed by X-ray diffraction (XRD) and scanning electron microscopy (SEM) in **Figure S1** and **Figure S2**a, b. We first deposited MAPbI$_3$(Cl) on the mesoporous TiO$_2$ (fluorine-doped tin oxide (FTO)/compact-TiO$_2$/meso-TiO$_2$) in ambient air for studying the atmospheric effect. After preparation, the sample was immediately transferred into the measurement chamber, which was subsequently closed to ensure a dark environment.

The atmosphere was controlled to simulate the work flow of a typical device fabrication (Figure 1b). First, E_f was acquired in ambient air. Then the chamber was pumped down slightly to 10^3 Pa using a rough pump and subsequently vented with dry N$_2$ to simulate transferring the sample inside a N$_2$-filled glovebox. In the next step, the chamber was pumped down to a high vacuum (10^{-3} ~ 10^{-4} Pa) by a turbo molecular pump. Because Kelvin probe measurements are sensitive to chamber vibration which causes substantial noise, measurement in vacuum is started after the rotation speed of turbo molecular pump is stabilized. This step is to simulate the transferring of the sample inside a vacuum chamber for the deposition of other functional layers. After about 60 min in vacuum, the chamber is filled with dry N$_2$ again to resemble the situation of taking out the device from a deposition chamber into the glovebox. Finally, air is introduced inside the chamber, which corresponds to transferring of the device

outside the glovebox. The sample is kept in dark at room temperature during the whole procedure to avoid any SPV effect.

In Figure 1c, evolution of the MAPbI$_3$(Cl) surface E_f is plotted against the different atmospheres. E_f of −4.6 eV (with respect to the vacuum level) was found in air after sample preparation. After replacing air with dry N$_2$, E_f maintained its previous level (–4.7 eV), implying that rough pumping and N$_2$ atmosphere has little effect on the energy level. This is consistent with the reported negligible adsorption of N$_2$ on the perovskite[8]. However, after further pumping down the chamber to $10^{-3} \sim 10^{-4}$ Pa, E_f drastically up-shifts to about −3.9 eV. As a reference, VBM and CBM of MAPbI$_3$(Cl) were measured by ultraviolet photoemission spectroscopy and inverse photoelectron spectroscopy (**Figure S3**a). The position of the band edges relative to the vacuum level are herein assumed to be consistent in all atmospheres since no significant difference of these levels was observed between ambient air and ultrahigh vacuum from earlier studies[15,21,22]. Accordingly, E_f of MAPbI$_3$(Cl) in high vacuum is about 0.2 eV below CBM, indicating a transition to a strong *n*-type character.

As the next step, the chamber was vented with dry N$_2$. Again, little effect was observed and E_f remained at its previous level of −3.9 eV. Finally, air was blown into the chamber. E_f moved gradually away from the CBM, and stabilized at −4.1 eV, thereby maintaining its *n*-doped feature. Heating the sample in ambient air, however, restored E_f fully to its initial value. Subsequent pumping into high vacuum reproduces the heavy *n*-doped character (**Figure** S4a). The doping and de-doping is reproducible by cycling between air and vacuum, implying that vacuum-induced doping is related with a reversable physical process rather than a permanent chemical change. In addition, no difference is found whether a mesoporous TiO$_2$ or compact TiO$_2$ is adopted as the substrate (Figure S4b).

The atmospheric effect on the E_f position is also studied for MAPbI$_3$(Cl) deposited on PEDOT:PSS. As shown in Figure 1d, after preparation, the surface E_f is −4.9 eV in ambient air. Purging the air in the chamber with N$_2$ does not induce obvious change. Similar to

MAPbI$_3$(Cl) deposited on TiO$_2$, however, E_f shifts toward the CBM after pumping the chamber to high vacuum, stabilized at about -4.2 eV. Venting the chamber back to N$_2$ does not affect the E_f position. Exposing the sample to air down-shifts E_f gradually away from the CBM.

To investigate whether the E_f shift in vacuum is specific to MAPbI$_3$(Cl) only, other perovskite formulations commonly used in the photovoltaic application are examined. As shown in **Figure 2**, E_f of the pure MAPbI$_3$ without adding Cl shows the same trend, i.e., shifting toward the CBM under vacuum. Doping KI into MAPbI$_3$ has been found to benefit device stability[23]. Nevertheless, on the KI-doped MAPbI$_3$, E_f also shows a drastic shift from the mid-bandgap to the CBM in vacuum. We then substitute the anion from iodine to bromine (MAPbBr$_3$), the cation from methylammonium to formamidinium (FAPbI$_3$, FAPbBr$_3$) and Cs (CsPbBr$_3$), or mixed halides (FAPbI$_{0.85}$Br$_{0.15}$) and cations ((Cs$_{0.05}$FA$_{0.54}$MA$_{0.41}$)Pb(I$_{0.98}$Br$_{0.02}$)$_3$). XRD patterns of the samples and UPS spectra for determining the transporting levels are provided in Figure S1 and Figure S3. All the formulations exhibit an E_f up-shift, indicating the transition from an intrinsic semiconductor to a more *n*-type semiconductor.

The results above imply that the *n*-type transition from air to vacuum atmosphere could be a universal property for lead halide perovskites. We propose that the transition could be related with the defect formation in the perovskite and the passivation effect from species in ambient air based on the findings from previous studies. First of all, the spin-coating and post-annealing of the perovskite would generate a substantial number of defects in the thin film. Particularly, among the various types of defects, halide vacancies were found to be readily created due to their low formation energy[8,24]. First-principle modelling has indicated that halide vacancies create trap states close to the CBM, which could function as donors[4,25]. Nevertheless, oxygen in air could bond to the perovskite forming superoxide to passivate the defects[8,26]. Water molecules in air have also been suggested to form a hydrate phase passivating the perovskite surface[27]. The 'self-healing' effect is reported to restore the

perovskite crystal structure, moving E_f to the mid-bandgap[8]. We proposed here that when being pumped into high vacuum, oxygen and water initially adsorbed in the film may desorb through grain-boundaries and pin-holes, exposing the defective crystal structure[9]. In the meantime, decomposition may extract more volatile species from the perovskite in vacuum. For example, $MAPbI_3$ is known to undergo decomposition in vacuum, forming volatile products such as CH_3NH_2, HI, NH_3 and CH_3I[28,29]. As a result, the remaining perovskite becomes more Pb^{2+} rich and I^- deficient, which has been reported to n-dope the film[3,30]. To verify this assumption, we reduce the post-annealing time during sample preparation to suppress defect formation. Indeed, the film is observed to be less n-type in both air and vacuum (Figure S4c). Similarly, defect induced self-doping could have also occurred in other types of lead halide perovskites under vacuum[31]. Finally, filling the chamber with air restores E_f gradually, which could be attributed to re-adsorption of oxygen and water. The initial value, however, is not fully restored even after hours of storage in the dark. This could be due to (1) re-adsorption of oxygen and water is limited by their slow diffusion into the film; (2) formation of a hydrate phase on the surface prevents further oxygen diffusion into the film. Heating the sample, instead, restores the E_f completely (Figure S4a), by evaporating the water-film barrier on the surface and accelerating intercalation of oxygen into the bulk. We note that to fully determine the mechanism of the energy level transition in vacuum, further studies on the physicochemical dynamics of adsorption and desorption of air species, and the doping distribution inside the film is needed. Also, it will be highly interesting to further investigate the atmospheric effect on perovskites based on lead-free formulations and lower dimensional structures.

2.3. Energy Level Alignment in Air

E_f obtained from Kelvin probe measurements in dark represents the energy level on the very surface of the sample. Its relative position to the vacuum level may not, however, preserve

through the bulk of the film towards the bottom interface. Three major components may contribute to the full energy-level landscape[32]: (1) band bending at the bottom interface, formed by the charge depletion; (2) band bending at the surface, induced by surface defect states; (3) interfacial dipoles due to physical or chemical interactions.

To probe the energy level beneath the MAPbI$_3$(Cl) surface, we first examine whether there is band bending that extends from the bottom interface. This is achieved by measuring E_f as a function of the perovskite film thickness. By varying the precursor solution concentration and spin-coating rate, we were able to vary the MAPbI$_3$(Cl) film thickness from 150 nm to 1 μm. Note that it is difficult to achieve a film with a thickness below 150 nm while ensuring a good film quality. The SEM images and XRD of the samples are shown in Figure S2c, d and Figure S1. In **Figure 3**a, surface E_f is plotted as a function of the perovskite thickness. Before MAPbI$_3$(Cl) deposition, E_f of TiO$_2$ is found at about −4.4 eV, consistent with the reported value[21]. After MAPbI$_3$(Cl) deposition, no significant variation of the E_f is found across all the thickness, which lies at about −4.5 eV, close to E_f of the substrate. A similar trend is found for MAPbI$_3$(Cl) on PEDOT:PSS in Figure 3b. The perovskite E_f keeps at about −4.9 eV, which is close to E_f of PEDOT:PSS.

To detect any possible band bending at thinner thickness than 150 nm, SPV is further studied. Illuminating the semiconductor with a supra-bandgap excitation generates free carriers within the light penetration depth. If electrons and holes are separated by, for example, the built-in field within a band bending region, a surface potential change (i.e. SPV) will be observed[20].

It is essential to determine first which interface could contribute to SPV. If the thickness of a semiconductor is larger than the light absorption depth and carrier diffusion length, SPV would be solely contributed by the illuminated surface. However, for MAPbI$_3$(Cl) studied here, a long carrier diffusion length of about 1.6 μm was estimated[18]. The substantially longer diffusion length than the film thickness implies that photocarriers may diffuse beyond

the illuminated region and travel to the opposite interface. SPV induced by illuminating the sample top surface hence may include contribution from not only the surface, but also charge separation at the bottom interface[20].

To confirm whether photocarriers can travel throughout the film, SPV is compared by selectively exciting the surface and bottom interface[20]. As illustrated in **Figure 4**a, in the case where photocarriers excited at one interface of the semiconductor do not travel to the other, SPV induced by the top and bottom illumination would be independent to each other, that is,

$$SPV_{top} + SPV_{bottom} \approx SPV_{top+bottom} \qquad (1)$$

where, SPV_{top}, SPV_{bottom}, and $SPV_{top+bottom}$ correspond to SPV excited by illuminating the top, bottom and both sides of the sample respectively. On the other hand, in the case where the carrier diffusion length exceeds the film thickness, both interfaces would contribute to the SPV regardless of which interface is excited (Figure 4b), thereby,

$$SPV_{top} \approx SPV_{bottom} \approx SPV_{top+bottom} \qquad (2)$$

To distinguish these two cases, we first study the 1 μm-thick $MAPbI_3(Cl)$ deposited on TiO_2 in ambient air. LEDs emitting at 627 nm are placed above and below the sample for generating photocarriers at the surface and bottom interface (Figure 1a). This wavelength does not excite SPV in the bare TiO_2 due to its large bandgap (~3.3 eV)[22], allowing us to study only the perovskite layer. To prevent light from penetrating to the opposite interface, illumination is kept at a low intensity of 0.2 mW cm^{-2} (penetration depth of approximately 290 nm)[18]. As shown in Figure 4c, SPV by illumination from the top, bottom or both sides are compared. The same SPV of −0.20 V are found for bottom and top-plus-bottom illumination, while the top illumination gives a close value of −0.14 V with the same sign (the negative sign is defined as negative charges moving towards the bottom). This result is

consistent with Eq. (2), implying that photocarriers have travelled through the film to the other interface.

Because photocarriers can travel throughout the film, charge separation at either the top surface or bottom interface can contribute to SPV. To determine at which interface charge separation has occurred, intensity of the top and bottom illumination is controlled. It is found that under an increasing light intensity, SPV increases monotonically before saturation (**Figure S5**a, b). A strong illumination of larger than 5 mW cm^{-2} is necessary to achieve SPV saturation for top illumination, while only about 0.2 mW cm^{-2} is sufficient for the bottom illumination. This implies that SPV is mainly contributed by charge separation at the bottom interface, thereby a stronger top illumination is required to get enough photocarriers reaching the bottom interface where the charges are separated. As a further proof, by illuminating only the top surface at a fixed light intensity, SPV decreases as the perovskite film thickness increases (Figure S5c, d). As the travelling distance increases, more photocarriers would undergo recombination before reaching the bottom interface, thereby lessening the SPV.

Next, we study what has caused the charge separation at the bottom (TiO$_2$/MAPbI$_3$(Cl)) interface. One possibility is the existence of band bending that induces charge separation. However, since the E_f of MAPbI$_3$(Cl) matches that of the TiO$_2$ substrate (Figure 3a), a band bending at the bottom interface would indicate a band bending at the surface with an opposite direction (diagram in **Figure S6**). Such a scenario would lead to an opposite SPV by top and bottom illumination, contradicting the results in Figure 4c, which shows the same sign of SPV. Alternatively, we propose that the SPV is induced by electron transfer from the perovskite to TiO$_2$. TiO$_2$ is a strong electron acceptor. Electron transfer from MAPbI$_3$ to TiO$_2$ was found to happen ultrafast upon excitation[33]. Owing to the low-lying VBM of TiO$_2$, holes are blocked and reside in the perovskite layer. Charge separation thus gives rise to a negative SPV, consistent with our observation. The corresponding energy diagrams are illustrated in Figure 4d.

In contrast to TiO_2, the highly conductive PEDOT:PSS has no significant barrier for extraction of both electrons and holes[34]. Therefore, the existence of any band bending at the bottom interface would be revealed in the SPV. 1 μm-thick $MAPbI_3(Cl)$ deposited on PEDOT:PSS is studied in ambient air. As shown in Figure 4e, even under intensive excitation (10 mW cm^{-2}), no significant SPV is observed by both top or bottom illumination. The result thus suggests a negligible band bending throughout the perovskite in ambient air. The corresponding energy diagrams are illustrated in Figure 4f.

In a recent study by Li et al.[30], an intrinsic carrier density of lower than 10^{13} cm^{-3} was determined by Hall measurements on $MAPbI_3$. At such a low doping profile, the depletion length at the electrode contact is estimated to be hundreds of microns, much larger than the typical perovskite film thickness[35]. Therefore, the band bending cannot reach saturation within the film thickness and the obsered band bending is insignificant[36]. Furthermore, little difference of E_f between the perovskite surface and substrate indicates a negligible dipole at the interfaces and thereby the contact follows the vacuum-level-alignment model.

2.4. Energy Level Alignment in Vacuum

We next examine the energy level alignment in vacuum. The thickness dependent E_f is shown in Figure 3. It is found that on TiO_2, the perovskite E_f remains constant across all the thickness from 150 nm to 1 μm, lying at about -3.9 eV. On PEDOT:PSS, E_f is pinned at about -4.1 eV. Both exhibit a highly n-type character independent of the thickness.

The SPV effect is further investigated in vacuum. In contrast to the case in air, no significant SPV is observed for $MAPbI_3(Cl)$ deposited on either TiO_2 or PEDOT:PSS (Figure 4c, e). The diminished SPV can be attributed to the transition of the perovskite from intrinsic to heavy n-type. Reported by Huang et al., for $MAPbI_3$ with E_f located 0.3 eV below CBM, which is similar to our samples herein, a carrier density on the order of $10^{17} \sim 10^{18}$ cm^{-3} was estimated[3]. At such a high doping concentration, photocarriers would undergo recombination

rapidly before diffusing into the bulk, thereby diminishing the SPV effect (Figure 4d, f).

Nevertheless, we note that surface band bending may play only a minor role. Previous studies

that probed the VBM on the very surface by ultraviolet photoemission spectroscopy and

deeper into the bulk by hard-x-ray photoelectron spectroscopy have not shown significant

difference on MAPbI$_3$[22,37].

Doping of the perovskite in vacuum could have occurred only on the film surface or

extended throughout the bulk. To distinguish these two cases, photoluminescence

characteristics are examined, which reveals the local information where the excitation light

penetrates. The static-state photoluminescence before and after exposure in vacuum for 1 h

(measured immediately after transferring the sample out to air after venting the chamber) are

compared. As shown in **Figure 5**a, the photoluminescence intensity decreases by 80 % after

vacuum exposure, which can be attributed to the highly doped feature of the film. Next, we

compared the transient photoluminescence by illuminating a 1-µm-thick MAPbI$_3$(Cl) sample

from the surface and bottom interface with a 400-nm-wavelength laser (light penetration

depth about 50 nm)[18]. As shown in Figure 5b, c, after exposure in vacuum, the average

lifetime dramatically decreased from 58 ns to 37 ns for surface illumination, and from 67 ns to

33 ns for bottom illumination. The reduction in lifetime indicates an accelerated charge

recombination due to doping. The photoluminescence decay is further divided into a fast and

slow component which are contributed by the surface and bulk regions of the sample (fitted to

a double exponential decay function). For both surface and bottom illumination, lifetime of

the fast and slow decay is reduced by about half after sample exposure in vacuum (Table S1).

The result implies that the perovskite is doped throughout the film thickness. We propose that

the passivating oxygen and water deep inside the film may desorb through pinholes and grain

boundaries when exposed in vacuum. As a result, MAPbI$_3$(Cl) is self-doped by its defects

throughout the film thickness.

At a highly doped state, band bending would occur at the bottom interface for establishing Fermi level alignment with the substrate to reach equilibrium. The resultant depletion thickness (W_D) can be computed from Eq. (3) assuming a one-sided abrupt junction:

$$W_D = \sqrt{\frac{2\varepsilon\varepsilon_0}{qN}(\Delta V)} \qquad (3)$$

where ε (= 32) is the relative dielectric constant of the perovskite film[38], ε_0 is the vacuum permittivity and q is electron charge. ΔV is the built-in voltage determined by the difference of the substrate work function and semiconductor Fermi level. N is the free carrier density, which is assumed to be $10^{17} \sim 10^{18}$ cm^{-3} for the n-doped perovskite as reported[3]. For MAPbI$_3$(Cl) on TiO$_2$, ΔV is about 0.5 V estimated from the energy levels in Figure 3a. The depletion thickness is calculated to be 42 ~ 133 nm. Similarly, the depletion thickness is estimated to be 53 ~ 168 nm for MAPbI$_3$(Cl) on PEDOT:PSS where $\Delta V \approx 0.8$ V. These results explain why a negligible band bending is observed in the thickness-dependent E_f in Figure 3, where the perovskite thickness is beyond 150 nm. The calculated depletion thickness is also in line with the band bending thickness reported in the vacuum-deposited MAPbI$_3$ by Olthof and Meerholz [7].

2.5. Implications on the Photovoltaic Performance

Transition of the doping character should affect the photovoltaic property of the perovskite. To confirm it, photocurrent is compared on MAPbI$_3$ before and after vacuum exposure using the conductive atomic force microscopy (c-AFM) (Figure 5d). As shown in Figure 5e, f and **Figure S7**a-c, the photocurrent is reduced by about half after exposure in vacuum, which can be attributed to an increase of charge recombination in a heavily doped film. Reduction of photocurrent is even more obvious on FAPbI$_3$, which gives a higher base photocurrent due to its smaller bandgap (Figure S7d-h). In addition, the distribution of photocurrent is uniform

inside the grain and at the grain boundaries, indicating that the doping occurs not only at the more defective grain boundaries but also within the grain.

Impact of the vacuum-induced doping is further examined in a complete device structure (FTO/compact-TiO$_2$/meso-TiO$_2$/MAPbI$_3$/Carbon). We employ carbon as the back electrode instead of metals to avoid any unwanted doping effect from vacuum exposure prior to device characterization. The doctor-bladed carbon paste in ambient air is highly porous (Figure S2e) providing paths for gas extraction from the perovskite layer under vacuum. The sample is placed in the chamber to allow *in situ* measurements (Figure 5g). As shown in Figure 5h, the dark current increases dramatically under vacuum indicating an increase of the free carrier concentration. We note that the shifted zero-point of the curve in air can be attributed to device hysteresis due to ion migration under the electric field[39]. In vacuum, however, the much-larger free-carrier current covers the hysteresis current and the zero-point returns to zero bias. On the other hand, the photocurrent drops by about half in vacuum under illumination (Figure 5i). This is consistent with the c-AFM result. The open-circuit voltage decreases slightly. The resultant degraded device performance can be attributed to the accelerated charge recombination as further discussed below. Current scans are also performed in dry N$_2$, low vacuum (10^2 Pa) and high vacuum ($10^{-3} \sim 10^{-4}$ Pa) to confirm that the current shift only occurs under high vacuum (Figure S7i), consistent with the trend of E_f shift in Figure 1. Photocurrent is also acquired under a solar simulator after transferring the sample out to the ambient air. However, only a slight decrease of the photovoltaic performance is observed compared to the device before vacuum exposure (Figure S7j). This may be attributed to the accelerated intercalation of oxygen under the strong light in air, thereby diminishing the vacuum effect[40].

To further confirm that the photocurrent drop is caused by the doping of the full perovskite layer, the carbon-electrode-based device is simulated by tuning the doping concentration of the perovskite from 10^{10} cm^{-3} to 10^{18} cm^{-3}, corresponding to a shift from intrinsic to highly *n*-

doped. A dramatic reduction of the photocurrent and a slight decrease of the open-circuit voltage at doping concentrations larger than 10^{16} cm^{-3} (**Figure S8**a) is in line with the experimental results in Figure 5i. Furthermore, doping only the perovskite surface does not reproduce the experimental results, corroborating the assumption that the bulk of perovskite is doped in vacuum (Figure S8b). The device structure with a gold electrode is also simulated (Figure S8c). A similar trend showing a deteriorated photovoltaic performance is found under heavy doping, which can be attributed to the screened built-in field (**Figure S9**a-d) and an increase of charge recombination (Figure S9e, f) in the heavily doped perovskite. Therefore, the results suggest that a heavily-doped profile in the perovskite should be avoided in order to obtain high photovoltaic performance.

3. Conclusion

In summary, the impact of atmosphere on the energy level alignment of MAPbI$_3$(Cl) is investigated by subjecting the sample to the typical environments involved in device fabrication processes, i.e., the ambient air, dry N$_2$ and vacuum. It is found that in air, MAPbI$_3$(Cl) appears as an intrinsic semiconductor. The energy levels at the substrate interface follows the vacuum-level-alignment. After pumped into vacuum, however, the perovskite quickly becomes n-type with its E_f shifting toward CBM. The energy level diagrams are depicted in **Figure 6**. Transferring the sample to N$_2$ does not change the energy level observed in the previous atmosphere. Furthermore, vacuum-induced n-doping is found to deteriorate the photovoltaic performance of the device. Our work highlights the importance of atmospheric control during perovskite device fabrication to avoid unintended doping. It is also noted that many studies in the literature to date did not distinguish the possible energy level change of the perovskite in their specific characterization atmospheres. The vacuum-induced n-doping of lead halide perovskites revealed herein thus urges a re-examination on the correlation of the energetics measurements with the real-world devices.

References

[1]   A. K. Jena, A. Kulkarni, T. Miyasaka, *Chem. Rev.* **2019**, *119*, 3036.

[2]   P. K. Nayak, S. Mahesh, H. J. Snaith, D. Cahen, *Nat. Rev. Mater.* **2019**, *4*, 269.

[3]   Q. Wang, Y. Shao, H. Xie, L. Lyu, X. Liu, Y. Gao, J. Huang, *Appl. Phys. Lett.* **2014**, *105*, 163508.

[4]   W.-J. Yin, T. Shi, Y. Yan, *Appl. Phys. Lett.* **2014**, *104*, DOI http://dx.doi.org/10.1063/1.4864778.

[5]   E. M. Miller, Y. Zhao, C. C. Mercado, S. K. Saha, J. M. Luther, K. Zhu, V. Stevanović, C. L. Perkins, J. van de Lagemaat, *Phys. Chem. Chem. Phys.* **2014**, *16*, 22122.

[6]   P. Schulz, L. L. Whittaker-Brooks, B. A. MacLeod, D. C. Olson, Y.-L. Loo, A. Kahn, *Adv. Mater. Interfaces* **2015**, *2*, 1400532.

[7]   S. Olthof, K. Meerholz, *Sci. Rep.* **2017**, *7*, 40267.

[8]   R. Brenes, C. Eames, V. Bulović, M. S. Islam, S. D. Stranks, *Adv. Mater.* **2018**, *30*, 1706208.

[9]   H.-H. Fang, S. Adjokatse, H. Wei, J. Yang, G. R. Blake, J. Huang, J. Even, M. A. Loi, *Sci. Adv.* **2016**, *2*, DOI 10.1126/sciadv.1600534.

[10]   M. Anaya, J. F. Galisteo-López, M. E. Calvo, J. P. Espinós, H. Míguez, *J. Phys. Chem. Lett.* **2018**, *9*, 3891.

[11]   Y. Tian, M. Peter, E. Unger, M. Abdellah, K. Zheng, T. Pullerits, A. Yartsev, V. Sundström, I. G. Scheblykin, *Phys. Chem. Chem. Phys.* **2015**, *17*, 24978.

[12]   Y. Cheng, F. So, S. W. TSANG, *Mater. Horiz.* **2019**.

[13] Z. Wu, Z. Liu, Z. Hu, Z. Hawash, L. Qiu, Y. Jiang, L. K. Ono, Y. B. Qi, *Adv. Mater.* **2019**, *0*, 1804284.

[14] A. Zohar, N. Kedem, I. Levine, D. Zohar, A. Vilan, D. Ehre, G. Hodes, D. Cahen, *J. Phys. Chem. Lett.* **2016**, *7*, 191.

[15] M. Ralaiarisoa, I. Salzmann, F.-S. Zu, N. Koch, *Adv. Electron. Mater.* **2018**, *4*, 1800307.

[16] A. Szemjonov, K. Galkowski, M. Anaya, Z. Andaji-Garmaroudi, T. K. Baikie, S. Mackowski, I. D. Baikie, S. D. Stranks, M. S. Islam, *ACS Mater. Lett.* **2019**, *1*, 506.

[17] A. Zohar, I. Levine, S. Gupta, O. Davidson, D. Azulay, O. Millo, I. Balberg, G. Hodes, D. Cahen, *ACS Energy Lett.* **2017**, *2*, 2408.

[18] Z. Liu, L. Qiu, E. J. Juarez-Perez, Z. Hawash, T. Kim, Y. Jiang, Z. Wu, S. R. Raga, L. K. Ono, S. (Frank) Liu, Y. B. Qi, *Nat. Commun.* **2018**, *9*, 3880.

[19] F.-S. Zu, P. Amsalem, I. Salzmann, R.-B. Wang, M. Ralaiarisoa, S. Kowarik, S. Duhm, N. Koch, *Adv. Opt. Mater.* **2017**, *5*, 1700139.

[20] L. Kronik, Y. Shapira, *Surf. Sci. Rep.* **1999**, *37*, 1.

[21] J. R. Harwell, T. K. Baikie, I. D. Baikie, J. L. Payne, C. Ni, J. T. S. Irvine, G. A. Turnbull, I. D. W. Samuel, *Phys. Chem. Chem. Phys.* **2016**, *18*, 19738.

[22] P. Schulz, E. Edri, S. Kirmayer, G. Hodes, D. Cahen, A. Kahn, *Energy Environ. Sci.* **2014**, *7*, 1377.

[23] D.-Y. Son, S.-G. Kim, J.-Y. Seo, S.-H. Lee, H. Shin, D. Lee, N.-G. Park, *J. Am. Chem. Soc.* **2018**, *140*, 1358.

[24] Q. A. Akkerman, G. Rainò, M. V Kovalenko, L. Manna, *Nat. Mater.* **2018**, *17*, 394.

[25] N. Liu, C. Yam, *Phys. Chem. Chem. Phys.* **2018**, *20*, 6800.

[26] X.-X. Ma, Z.-S. Li, *Appl. Surf. Sci.* **2018**, *428*, 140.

[27] A. M. A. Leguy, Y. Hu, M. Campoy-Quiles, M. I. Alonso, O. J. Weber, P. Azarhoosh, M. van Schilfgaarde, M. T. Weller, T. Bein, J. Nelson, P. Docampo, P. R. F. Barnes, *Chem. Mater.* **2015**, *27*, 3397.

[28] E. J. Juarez-Perez, L. K. Ono, M. Maeda, Y. Jiang, Z. Hawash, Y. B. Qi, *J. Mater. Chem. A* **2018**, *6*, 9604.

[29] E. J. Juarez-Perez, Z. Hawash, S. R. Raga, L. K. Ono, Y. B. Qi, *Energy Environ. Sci.* **2016**, *9*, 3406.

[30] P. Cui, D. Wei, J. Ji, H. Huang, E. Jia, S. Dou, T. Wang, W. Wang, M. Li, *Nat. Energy* **2019**, *4*, 150.

[31] A. García-Fernández, E. J. Juarez-Perez, S. Castro-García, M. Sánchez-Andújar, L. K. Ono, Y. Jiang, Y. B. Qi, *Small Methods* **2018**, *2*, 1800242.

[32] H. Ishii, K. Sugiyama, E. Ito, K. Seki, *Adv. Mater.* **1999**, *11*, 605.

[33] R. Long, W.-H. Fang, O. V Prezhdo, *J. Phys. Chem. C* **2017**, *121*, 3797.

[34] S. A. Mauger, L. Chang, C. W. Rochester, A. J. Moulé, *Org. Electron.* **2012**, *13*, 2747.

[35] I. D. Parker, *J. Appl. Phys.* **1994**, *75*, 1656.

[36] P. Bernier, G. Bidan, S. Lefrant, *Advances in Synthetic Metals: Twenty Years of Progress in Science and Technology*, Elsevier, **1999**.

[37] R. Lindblad, D. Bi, B. Park, J. Oscarsson, M. Gorgoi, H. Siegbahn, M. Odelius, E. M. J. Johansson, H. Rensmo, *J. Phys. Chem. Lett.* **2014**, *5*, 648.

[38] Q. Dong, Y. Fang, Y. Shao, P. Mulligan, J. Qiu, L. Cao, J. Huang, *Science (80-.).* **2015**, *347*, 967.

[39] A. Rizzo, F. Lamberti, M. Buonomo, N. Wrachien, L. Torto, N. Lago, S. Sansoni, R. Pilot, M. Prato, N. Michieli, M. Meneghetti, G. Meneghesso, A. Cester, *Sol. Energy Mater. Sol. Cells* **2019**, *189*, 43.

[40] W. Kong, A. Rahimi-Iman, G. Bi, X. Dai, H. Wu, *J. Phys. Chem. C* **2016**, *120*, 7606.
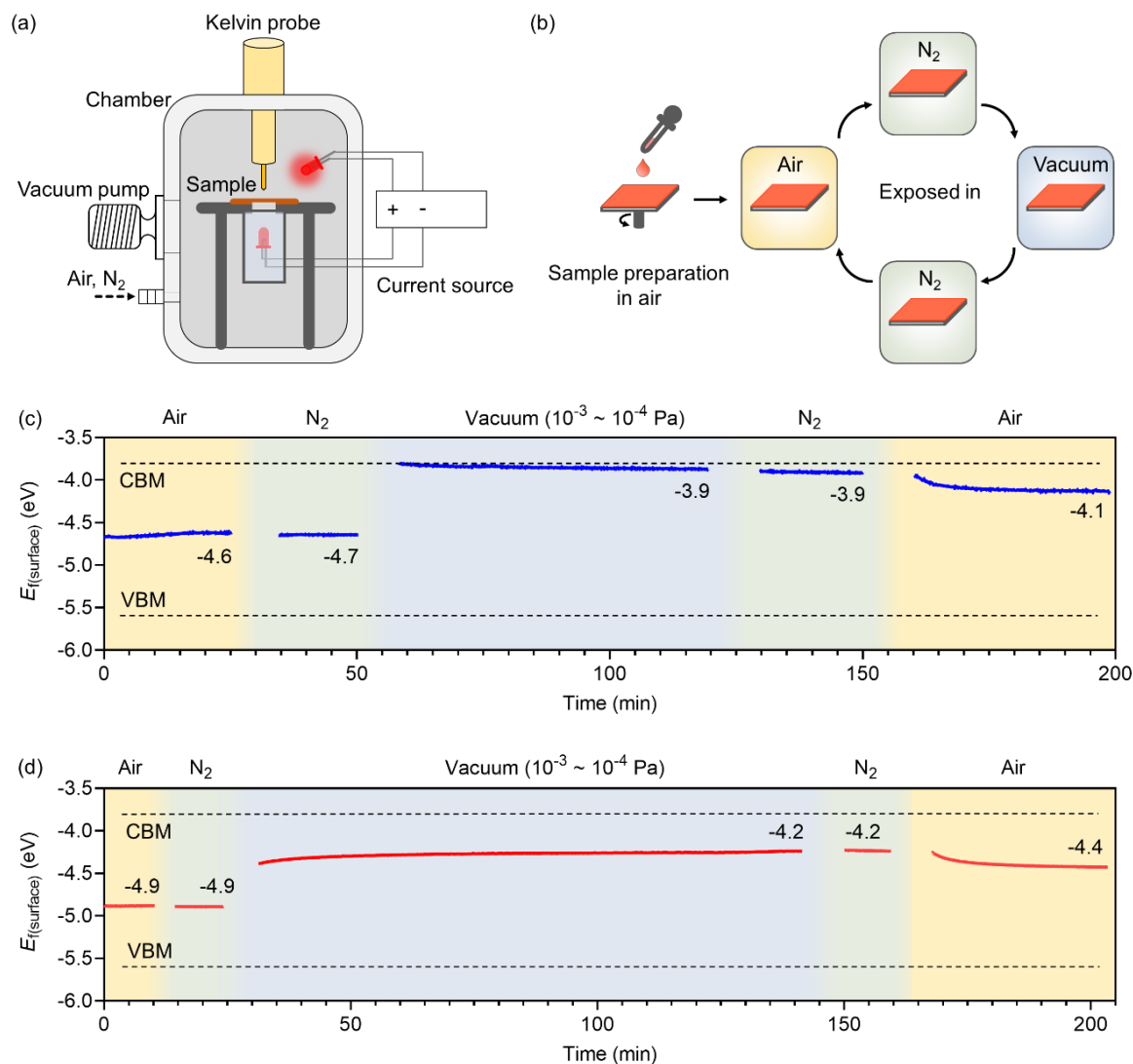
Figure 1. a) The Kelvin probe set-up inside a vacuum chamber. The turbo molecular pump provides a high vacuum of $10^{-3} \sim 10^{-4}$ Pa. The chamber can be vented with dry N_2 or ambient air through a gas valve. Two LED light sources are placed above and below the sample for inducing SPV. b) Measurement flow of the experiment: the perovskite thin film is prepared in ambient air, which is subsequently transferred into the Kelvin probe chamber for measurement while exposed sequentially to atmospheres of air, N_2, vacuum, then back to N_2 and air. c) Evolution of the surface E_f on FTO/compact-TiO$_2$/meso-TiO$_2$/MAPbI$_3$(Cl) under the atmospheres; d) Evolution of the surface E_f on ITO/PEDOT:PSS/MAPbI$_3$(Cl) under the atmospheres. During the whole process, the sample is kept in dark at room temperature. The MAPbI$_3$(Cl) layer is 800 nm thick. VBM and CBM are obtained from PES in Figure S3.
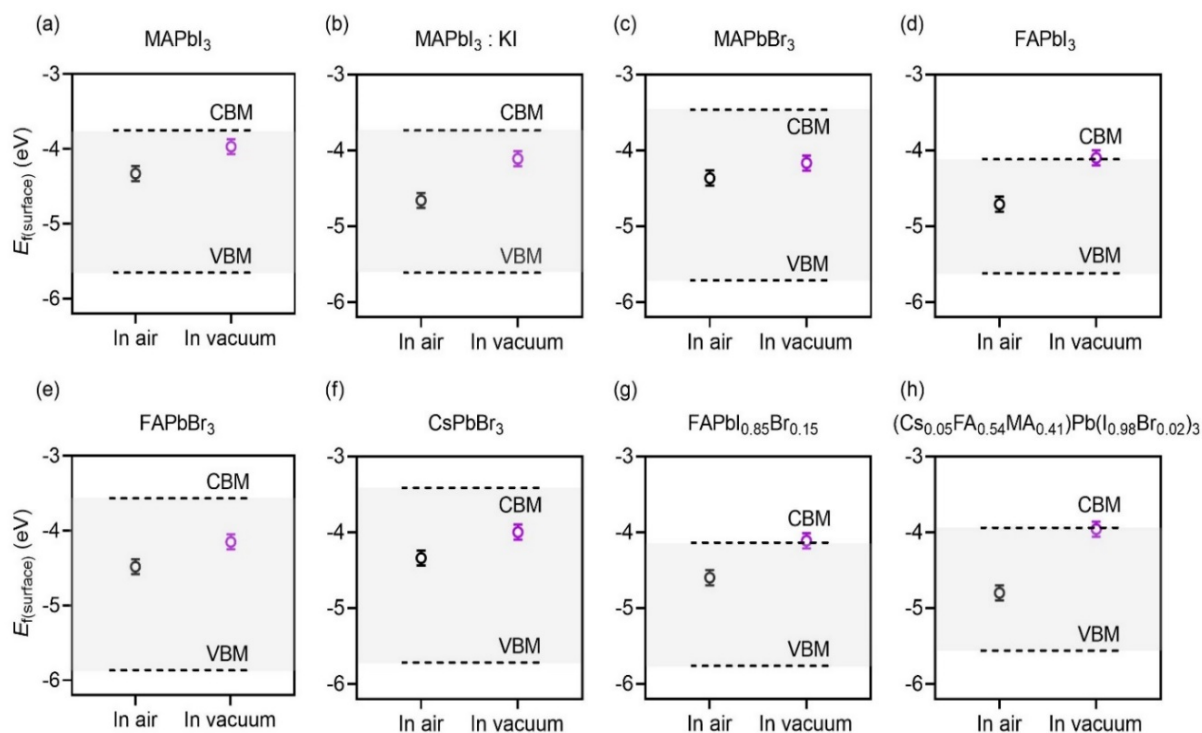
Figure 2. Surface E_f of other types of perovskites in air and vacuum. a) $MAPbI_3$ on meso-TiO_2, b) KI doped $MAPbI_3$ on meso-TiO_2, c) $MAPbBr_3$ on meso-TiO_2, d) $FAPbI_3$ on SnO_2, e) $FAPbBr_3$ on SnO_2, f) $CsPbBr_3$ on meso-TiO_2, g) $FAPbI_{0.85}Br0_{.15}$ on SnO_2, and h) $(Cs_{0.05}FA_{0.54}MA_{0.41})Pb(I_{0.98}Br_{0.02})_3$ on meso-TiO_2. The samples were subjected to air and high vacuum ($10^{-3} \sim 10^{-4}$ Pa) in dark. The VBM is obtained by UPS and CBM is calculated from the bandgap (Figure S9). The error bars are ± 0.1 eV.
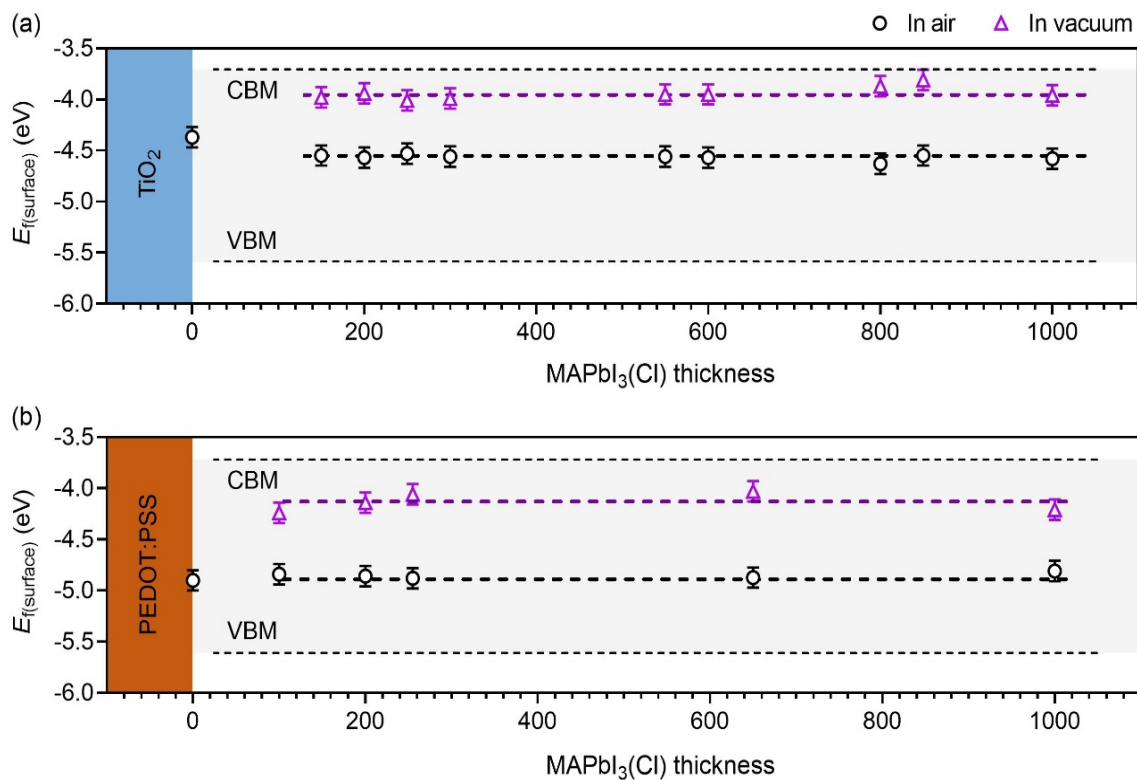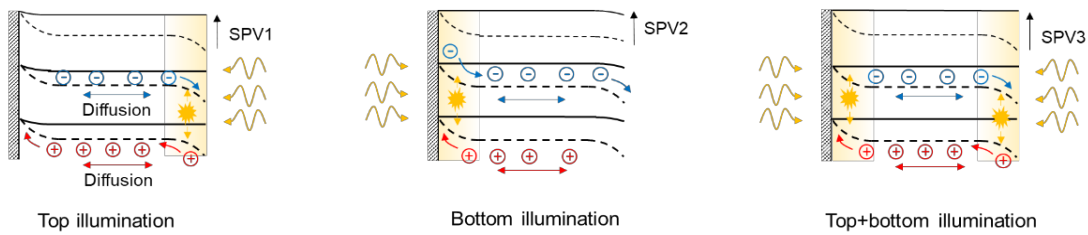
Figure 3. Thickness-dependent E_f on MAPbI$_3$(Cl). a) FTO/compact-TiO$_2$/meso-TiO$_2$/MAPbI$_3$(Cl) in air and in vacuum ($10^{-3} \sim 10^{-4}$ Pa). b) ITO/PEDOT:PSS/MAPbI$_3$(Cl) in air and in vacuum ($10^{-3} \sim 10^{-4}$ Pa). The error bars are ± 0.1 eV
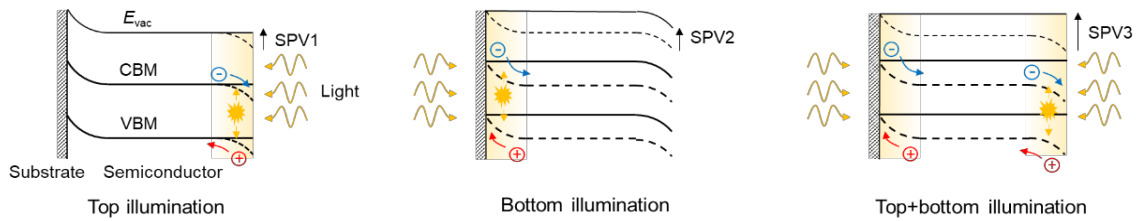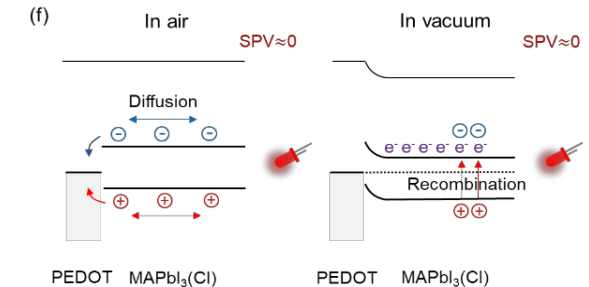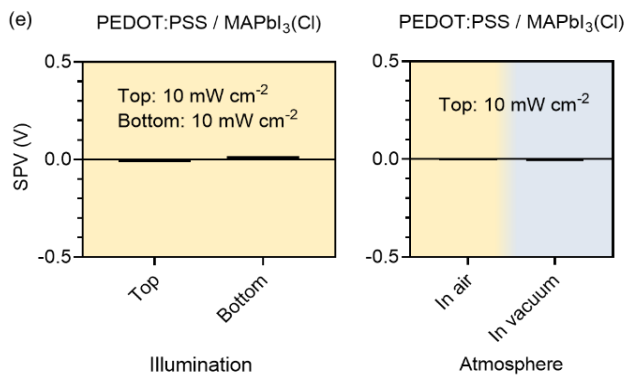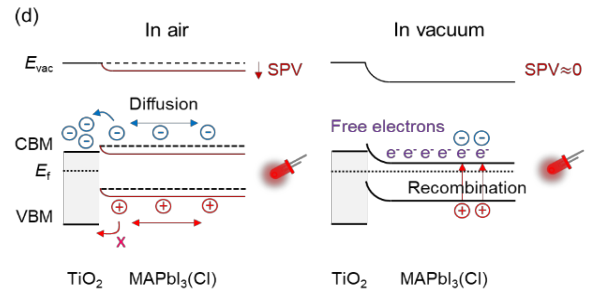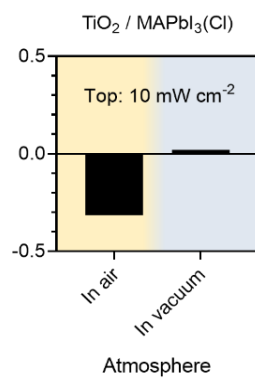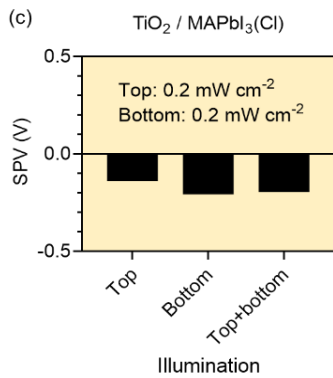
Figure 4. SPV on MAPbI₃(Cl). a) Assuming a semiconductor on a transparent substrate with a band bending at the top and bottom, if the carrier diffusion length is shorter than the semiconductor thickness, SPV excited by top and bottom illumination is independent to each other. b) If the carrier diffusion length is longer than the semiconductor thickness, both interfaces would contribute to the SPV upon either the top and bottom illumination. c) SPV on FTO/compact-TiO₂/meso-TiO₂/MAPbI₃(Cl) is compared by illuminating the sample from the top and bottom in air and in vacuum. d) The energy diagrams of MAPbI₃(Cl) on TiO₂ upon illumination. For comparison, the dashed lines indictate the energy levels in dark. Under illumination in air, charge transfer at the bottom interface leads to an energy level shift. e) SPV on ITO/PEDOT:PSS/MAPbI₃(Cl) is compared by illuminating the sample from the top and bottom in air and in vacuum. f) The energy diagrams of MAPbI₃(Cl) on PEDOT:PSS upon illumination.
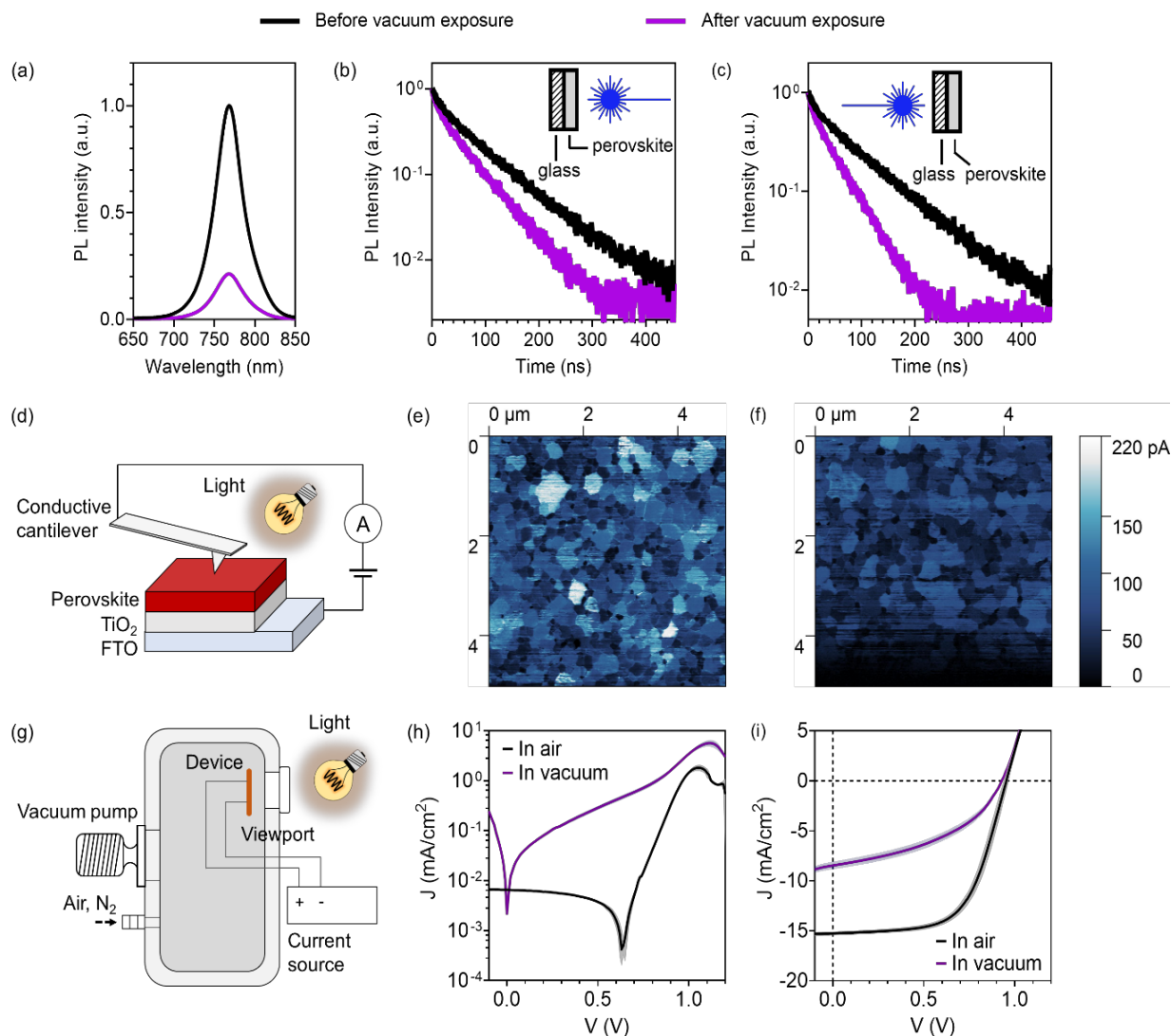
Figure 5. Photoluminescence and electrical characteristics of the perovskite. (a) Static-state photoluminescence intensity of MAPbI$_3$(Cl) on TiO$_2$. Transient photoluminescence characteristics before and after exposure in vacuum ($10^{-3} \sim 10^{-4}$ Pa, for 1 hr) are compared for the excitation laser incident on the (b) perovskite surface and (c) bottom interface. Thickness of the perovskite is 1 µm. Electrical characteristics of the perovskite. (d) c-AFM set-up for mapping the photocurrent on the perovskite. (e) Photocurrent mapping at short-circuit on FTO/compact-TiO$_2$/meso-TiO$_2$/MAPbI$_3$ before vacuum exposure. The height image is provided in Figure S20a. (f) Photocurrent mapping at short-circuit on FTO/compact-TiO$_2$/meso-TiO$_2$/MAPbI$_3$ after vacuum exposure. The height image is provided in Figure S20b. (g) Device of FTO/compact-TiO$_2$/meso-TiO$_2$/MAPbI$_3$/Carbon is loaded in the chamber to enable in-situ measurement in different atmospheres. (h) Dark current of the device in air and in vacuum ($10^{-3} \sim 10^{-4}$ Pa). (i) Photocurrent of the device in air and in vacuum ($10^{-3} \sim 10^{-4}$ Pa). The shaded areas of the curves define the standard deviation.
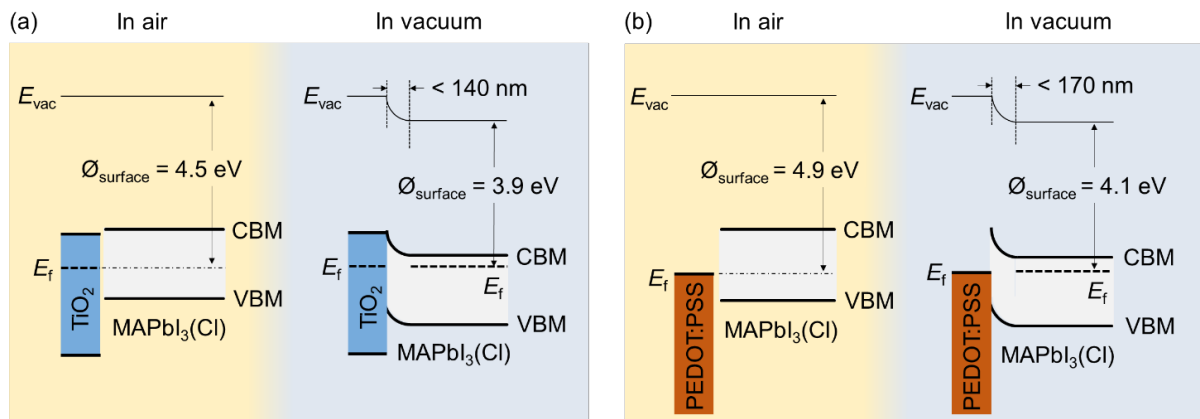
Figure 6. a) Energy level diagrams of MAPbI$_3$(Cl) on TiO$_2$ in air and vacuum. b) Energy level diagrams of MAPbI$_3$(Cl) on PEDOT:PSS in air and vacuum. In air, the substrate interface follows the vacuum-level-alignment. In vacuum, a band bending is located at the bottom interface, which is estimated to be within 140 nm and 170 nm on the TiO$_2$ and PEDOT:PSS substrates respectively.

The energy level alignment of the lead-halide perovskite thin film is studied subjected to a cycle of atmospheres relevant to industrial production. The atmospheric induced doping and de-doping is found to affect the photovoltaic property significantly. The impact of the environment implies careful control of the atmosphere is necessary for achieving the best device performance.

Z. Hu, Z. Liu, L. K. Ono, M. Jiang, S. He, D.-Y. Son, and Y. B. Qi*

Title The impact of atmosphere on energetics of lead halide perovskites